

Syntheses and Properties of the New Electron Transfer Sensitizers 4,2'-Pyrlogens

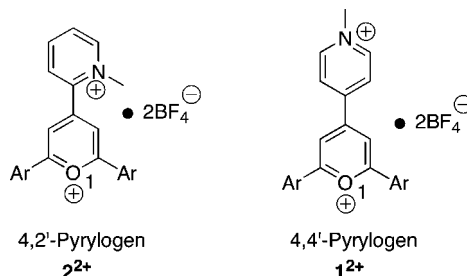
Edward L. Clennan* and Ajaya Kumar Sankara Warriar

Department of Chemistry, University of Wyoming, 1000 East University Avenue, Laramie Wyoming 82071

clennane@uwyo.edu

Received November 29, 2008

ABSTRACT



The syntheses and characterizations of the 4,2'-regioisomers of the dicationic pyrlogen electron transfer sensitizers are reported. The electrochemical and photophysical properties of these sensitizers are compared to the previously reported 4,4'-pyrlogens.

Photoinduced electron transfer (PET) reactions have become a standard tool in the synthetic chemist's bag of utensils.¹ The unique reactivities exhibited by open shell species generated in these reactions have provided access to synthetic transformations that are difficult or impossible to achieve by any other method.² Commercialization of PET reactions, however, are impeded by the cost associated with their low quantum yields. In many cases, the low efficiencies can be attributed to energy wasting return electron transfer (RET) that competes with the desired reaction.³

To suppress detrimental RET, we recently introduced 4,4'-pyrlogens, 1²⁺, as a new class of sensitizer.⁴ These sensitizers were designed to generate mutually repulsive radical-cations that would exhibit an increased rate of

diffusive separation thereby enhancing inhibition of RET. This new approach is an extension of the charge shift reaction⁵ which previously was restricted to singly charged sensitizers that generate nonattractive radical/radical-cation pairs. Although this approach was successful, RETs in these nonattractive radical/radical-cation pairs were far from completely eliminated and separation quantum yields significantly less than one were still observed.⁶ Consequently, efforts to extend this concept to dicationic sensitizers to generate mutually repulsive ions are warranted. Therefore, we report here the syntheses and characterizations of the previously unknown 4,2'-isomers, 2a-c²⁺, of the 4,4'-pyrlogens⁴ and their photophysical and electrochemical properties.

These new pyrlogens were synthesized as shown in Scheme 1.⁷ In the first step, condensation of two equivalents of a phenone, presumably via an α,β -unsaturated intermedi-

(1) Kravarnos, G. J. *Fundamentals of Photoinduced Electron Transfer*; VCH Publishers Inc.: Cambridge, UK, 1993.

(2) Ohkubo, K.; Iwata, R.; Miyazaki, S.; Kojima, T.; Fukuzumi, S. *Org. Lett.* **2006**, *8*, 6079–6082.

(3) Gould, I. R.; Moser, J. E.; Armitage, B.; Farid, S. *Res. Chem. Intermed.* **1995**, *21*, 793–806.

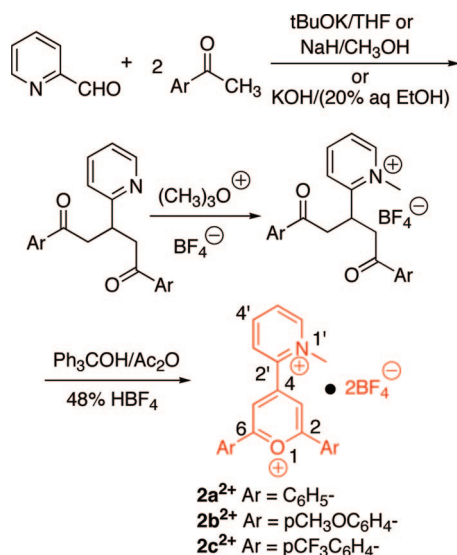
(4) Clennan, E. L.; Liao, C.; Ayokosok, E. J. *Am. Chem. Soc.* **2008**, *130*, 7552–7553.

(5) Gould, I. R.; Moser, J. E.; Armitage, B.; Farid, S.; Goodman, J. L.; Herman, M. S. *J. Am. Chem. Soc.* **1989**, *111*, 1917–1919.

(6) Todd, W. P.; Dinnocenzo, J. P.; Farid, S.; Goodman, J. L.; Gould, I. R. *J. Am. Chem. Soc.* **1991**, *113*, 3601–3602.

ate, generates a 1,5-diketone that is readily converted to the pyridinium ion with Meerwein's salt. Oxidative cyclization of the 1,5-diketo-pyridinium salt was best accomplished using in situ generated trityl cation in a mixture of acetic anhydride and 48% HBF₄.

Scheme 1. Syntheses of 4,2'-Pyrylogens



The spectral data, especially the appearance of a diagnostic two proton singlet for the pyrylium ring hydrogens at 8.68 ppm in **2a**²⁺, 8.30 ppm in **2b**²⁺, and 8.90 ppm in **2c**²⁺, and the disappearances of the carbonyl peak at 198.1 ppm (**2a**²⁺), 197.4 (**2b**²⁺), and 198.4 (**2c**²⁺) in the ¹³C NMR, and the CO stretch in the IR at 1684 cm⁻¹ (**2a**²⁺), 1672 cm⁻¹ (**2b**²⁺), and 1700 cm⁻¹ (**2c**²⁺) in the 1,5-dione precursor provides strong evidence for formation of the pyrylogen. (See Supporting Information for complete spectral data.) This was confirmed by an X-Ray structure of **2a**²⁺·2BF₄⁻ (Figure 1). A striking feature of the structure is the significant twist of the pyridinium ring (65.8°) out of the plane of the pyrylium cation in comparison to the 2- and 6-phenyl rings (2.5° and 10.7°). We attribute this to the steric interaction between the *N*-methyl group and the pyrylium ring rather than to crystal packing forces. For comparison, the pyridinium ring in **1**²⁺ is only twisted out of the pyrylium ring plane by 41.5°. This contention is also supported by calculations using the B3LYP/6-31G(d) model which predicts twist angles of 53.2°, 78.4°, 73.7°, 75.3°, 74.7°, and 78.6° for **1**²⁺, **2a**²⁺, the (ii), (io), and (oo) rotomers of **2b**²⁺, and **2c**²⁺, respectively.⁸ (See Supporting Information for more detailed computed structural data.)

Electrochemical Behavior. The 4,2'-pyrylogens in analogy to the closely related viologens exist in three readily accessible redox states as shown in Scheme 2. In both the 4,2'-pyrylogens, **2**²⁺, and *N*-methyl-2,6-diphenyl-4,4'-pyry-

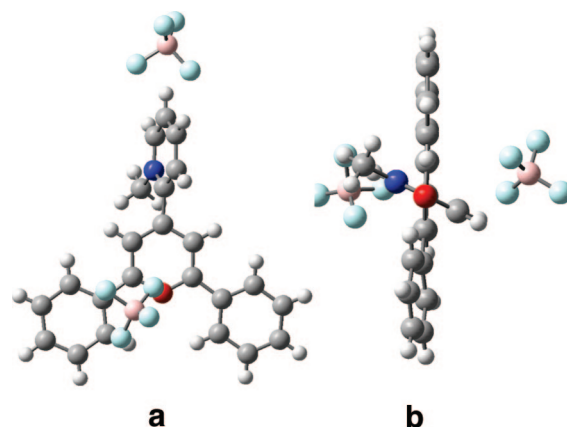
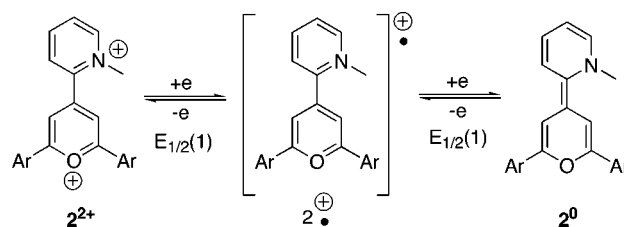


Figure 1. (a) Face-on and (b) edge-on perspectives of the X-Ray structure of **2a**²⁺.

logen **1**²⁺ regioisomers, the radical cations and the neutral redox partners are stable on the cyclic voltammetry (CV) time scale even at scan rates of 50 mV/sec. However, there are also very distinctive differences in the CV behavior of the two regioisomers. For example, the first reduction potential of **2a**²⁺ to form the radical cation is 110 mV cathodic of the first reduction of **1**²⁺. The reduction potentials (Table 1) to form the radical cations (E_{1/2}(1)) are also more sensitive to substituent effects in the 4,2'- (ρ = 0.92; r² = 0.9978) than in the 4,4'- (ρ = 0.34; r² = 0.9988) regioisomers.⁴ In addition, the 4,2' pyrylogen radical cations and neutral redox partners react rapidly with oxygen on the CV time scale even at 500 mV/sec while the 4,4'-regioisomer, **1**²⁺, is unreactive even at scan rates as slow as 50 mV/sec.

Scheme 2. Redox States of the 4,2'-Pyrylogens



To understand these differences, we have computationally examined all three redox states using the B3LYP/6-31G(d) model. With this model, **2a**²⁺ is 8.11 kcal/mol less stable than its isomer **1**²⁺ but **2a**^{•+} is 9.37 kcal/mol less stable than **1**^{•+}. These calculated energy differences require that the dication/radical-cation energy gap be 1.26 kcal/mol smaller for **1**²⁺ than for **2**²⁺ nearly identical to the 110 mV (2.53 kcal/mol) difference in reduction potentials. We suggest that the higher energies of **2a**²⁺ and **2a**^{•+} than their 4,4'-counterparts reflect the loss of delocalization energy in the more highly twisted 4,2'-isomers (i.e., the inter-ring dihedral angles in **2a**²⁺ (78.45°) and **2a**^{•+} (35.41°) are significantly larger than in **1**²⁺ (41.48°) and **1**^{•+} (3.91°)).

(7) Katritzky, A. R.; Adamson, J.; Elisseou, E. M.; Musumarra, G.; Patel, R. C.; Sakizadeh, K.; Yeung, W. K. *J. Chem. Soc., Perkin Trans. II* **1982**, 1041–1048.

The differences in sensitivity to substituent effects we attribute to a greater decrease in the positive charge upon

Table 1. Photophysical and Electrochemical Data for **1**, **2a–c**, and **3**

	1 ²⁺	2a ²⁺	2b ²⁺	2c ²⁺	3 ²⁺
$E_{1/2}$ (1) ^a	0.17	0.06	−0.08	0.22	−0.35
$E_{1/2}$ (2) ^a	−0.35	−0.41	−0.45	−0.34	−1.53
λ_F ^b	533	511	623	481	465
λ_P ^c	565	567	628	550	520
τ_P ^d	35.6 ± 0.2	39.5 ± 2	63.6 ± 8	19.6 ± 4	225 ± 3
$\Delta\lambda$ ^e	93	76	113	71	64
E (S ₁)	59	61	52	64	65 ^f
E (T ₁)	54	54	49	56	53 ^f
Φ_F	0.18 ± 0.01	0.54 ± 0.01	0.048 ± 0.01	0.44 ± 0.04	0.60 ^f

^a In volts vs SCE. ^b In nm at 298 K. ^c In nm in EtOH/HCl(g) at 77 K. ^d In milliseconds (ms) at 77 K in EtOH/HCl(g). ^e Stokes shift in nm. ^f Miranda, M. A.; Garcí'a, H. *Chem. Rev.* **1994**, *94*, 1063–1069. ^g 2,4,6-Triphenylpyrylium.

reduction in the pyrylium and aryl rings of the 4,2'- in comparison to the 4,4'-regioisomer. This is supported by decreases of the Mulliken atomic charges by 0.621 and 0.568 in the pyrylium and aryl rings upon reductions of **2a**²⁺ and **1**²⁺, respectively. Finally, the Mulliken spin densities are more localized in the pyrylium ring (0.63) of **2a**²⁺ but more evenly distributed in the pyridinium (0.49) and pyrylium ring (0.51) of **1**²⁺ which also explains the higher reactivity of **2a**²⁺ with oxygen (vide supra).

Chemical reductions of **2a–c**²⁺ with zinc dust in an acetonitrile slurry resulted in disappearance of the pyrylogen and appearance of long wavelength UV–vis bands as shown in Figure 2. We assign these new species to the radical cations, **2**²⁺. Unfortunately, TD-DFT calculations with B3LYP/6–31G(d) geometries of open shelled species that form charge transfer excited states similar to **2**²⁺ are well-known to be unreliable and cannot be used to verify these assignments.⁹ On the other hand, TD-DFT calculations with the B3LYP/6–31G(d) model with closed shell species are known to give excellent agreement with experimental UV–visible spectra. Indeed, the calculated wavelengths of the long wavelength absorbances of **2a**²⁺ (442 nm), **2b**²⁺ (518 nm), **2c**²⁺ (430 nm) are in excellent agreement with the observed values of 435 nm, 510 nm, and 410 nm, respectively. Consequently, the very poor agreement between the calculated λ_{MAX} for **2a**⁰ (595 nm, $f = 0.0907$; 467 nm, $f = 0.9597$), **2b**⁰ (572 nm, $f = 0.1008$; 510 nm, $f = 0.3979$), and **2c**⁰ (665 nm, $f = 0.1426$; 535 nm, $f = 0.6284$) and the experimental values in Figure 2 argue against a two electron chemical reduction and instead are consistent with our assignment of the UV–vis spectra of the Zn reduction products to the radical cations. In addition, treatment of both

1²⁺ and **2a**²⁺ under the same reducing conditions also generated single line ESR spectra with g-values of 2.0215 and 2.0038, respectively.¹⁰

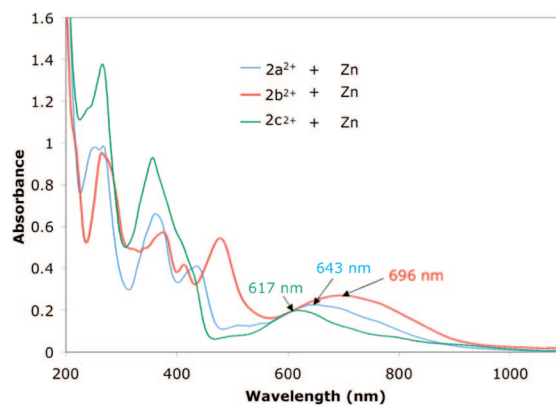


Figure 2. UV–visible spectra of zinc **2a–c**²⁺ reduction products.

The B3LYP/6–31G(d) geometries of the 3 redox states also establish the validity of the structural representations shown in Scheme 2. For example, the inter-ring distance, d_{42} , decreases from 1.499 to 1.442 to 1.392 Å in the series **2a**²⁺, **2a**⁺, and **2a**⁰ while the oxygen–carbon distance, d_{12} , increased from 1.355 to 1.368 to 1.385 Å. The inter-ring dihedral angle also dramatically decreases from 78.45 to 35.41 to 19.31°, consistent with an increase in the π bond order of bond 4–2'. The change in the hybridization at nitrogen evident in the structural representations in Scheme 2 is also consistent with the decrease in the dihedral angle >32°NCH₃ in **2a**²⁺ (178.63°), **2a**⁺ (168.00°), and **2a**⁰ (149.28°) and with the implied loss of aromaticity in the pyrylium and pyridinium ring along this redox series.

Photophysical Behavior. The UV–visible spectra of the pyrylogens and for 2,4,6-triphenylpyrylium tetrafluoroborate, **3**, are shown in Figure 3. The UV–vis spectra of the 4,4'-, **1**²⁺, and 4,2'-, **2a**²⁺, pyrylogens are very similar both exhibiting 3 bands with similar relative intensities and wavelengths. The oscillator strengths, however, are larger in **1**²⁺ than in **2a**²⁺ at the λ_{MAX} of all three bands. The long wavelength bands in all the pyrylogens are also bathochromic of the long wavelength band in **3** (i.e., λ_{MAX} **2b** > **1** > **2a** > **2c** > **3**).

All of the pyrylogens emitted both fluorescence and phosphorescence at the wavelengths listed in Table 1. The singlet energies were determined from the crossing points of the fluorescence and normalized absorption spectra. The triplet energies were estimated using the short wavelength onset of the phosphorescence spectra. The fluorescence quantum yields of the pyrylogens, Φ_{PY} , were determined in acetonitrile and compared to the fluorescence quantum yield of 9,10-diphenyl anthracene Φ_{DPA} using equation 1 in which A_{PY} and A_{DPA} are the absorbances at the excitation wavelength, n_{ACN} and $n_{Cyclohexane}$ are the refractive indices of the

(8) (ii), (io), and (oo) refer to rotameric isomers of **2b** involving the methoxy group. The o refers to the rotomer in which the methyl group points out toward the pyridinium ring and i to the rotomer in which the methyl group points in towards the pyrylium oxygen.

(9) (a) Zhang, D.; Telo, J. P.; Liao, C.; Hightower, S. E.; Clennan, E. L. *J. Phys. Chem.* **2007**, *111*, 13567–13574. (b) Drewu, A.; Head-Gordon, M. *J. Am. Chem. Soc.* **2004**, *126*, 4007–4016.

(10) Clennan, E. L.; Liao, C. unpublished results.

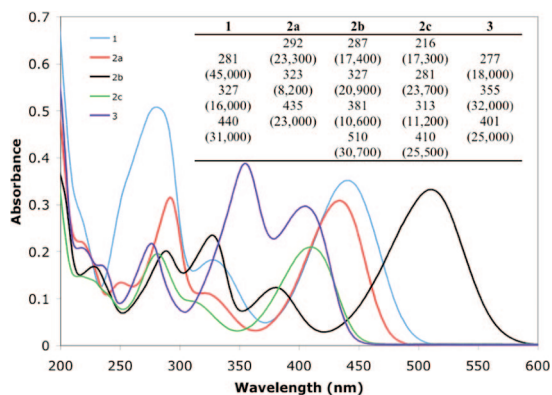


Figure 3. UV-vis spectra [$\lambda_{\text{MAX}}(\epsilon)$] for **1** (2.3×10^{-5} M), **2a** (2.29×10^{-5} M), **2b** (1.07×10^{-5} M), **2c** (8.5×10^{-6} M), and **3** (1.25×10^{-5} M).

solvents, and F_{PY} and F_{DPA} are the integrated emission areas.¹¹ The fluorescence quantum yields decrease as the singlet-triplet energy gap gets smaller consistent with an increase in the rate of intersystem crossing. The phosphorescence spectra were collected in an HCl gas saturated ethanol matrix at 77 K. Control experiments demonstrated that the pyrylogens were stable under these conditions. The relative quantum efficiencies estimated from the normalized integrated intensities of the phosphorescence spectra (**1**²⁺ 1.0; **2a**²⁺ 0.54; **2b**²⁺ 0.025; **2c**²⁺ 0.94) are smaller for the 4,2' than for the 4,4' pyrylogen. The ability of the p-methoxy substituent in **2b**²⁺ to reduce the intensity of phosphorescence was also noted previously in the 4,4'-regioisomer.²

$$\Phi_{\text{PY}} = \left[\frac{A_{\text{DPA}} F_{\text{PY}} (n_{\text{ACN}})^2}{A_{\text{PY}} F_{\text{DPA}} (n_{\text{Cyclohexane}})^2} \right] \Phi_{\text{DPA}} \quad (1)$$

Nanosecond laser flash photolysis (LFP) studies with **2a**²⁺ in 1,2-dichloroethane resulted in the observation of a prominent peak at 550 nm with a lifetime of $14 \pm 2 \mu\text{s}$ as shown in Figure 4. We have identified this transient as the

(11) Eaton, D. F. In *Handbook of Organic Photochemistry*; Scaiano, J. C., Ed.; CRC Press: Boca Raton, FL, 1989; Vol. 1, pp 231–239.

triplet based on the ability of oxygen to dramatically reduce its lifetime and the ability of bromobutane to enhance its intensity by approximately 30%. In addition, the intensities of similar transients observed in the LFP of **2b**²⁺ (appx. 625 nm; $\tau = 37 \pm 16 \mu\text{s}$) and **2c**²⁺ (530 nm; $\tau = 25 \pm 6 \mu\text{s}$) mirrored the intensities of their phosphorescence emissions.

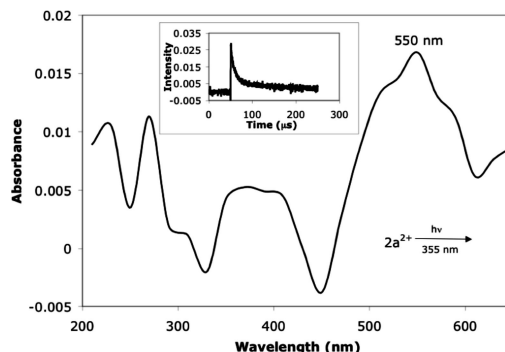


Figure 4. LFP Spectrum of **2a**²⁺ 4.7 μs after irradiation at 355 nm in 1,2-dichloroethane; (Inset) decay at 550 nm.

In conclusion, the 4,2'-pyrylogens all have low energy absorption bands that will allow irradiations of many reaction mixtures without concern about competitive absorption by substrates. In addition, their ease of reduction coupled with their excited-state energies provide potent oxidants that in the case of the S_1 state of **2c**²⁺ is capable of removing an electron from substrates with oxidation potentials as high as 3.0 eV. (reduction potentials: **1**²⁺ S_1 -2.73 eV, T_1 -2.51 eV; **2a**²⁺ S_1 -2.71 eV, T_1 -2.51 eV; **2b**²⁺ S_1 -2.18 eV, T_1 -2.04 eV; **2c**²⁺ S_1 -3.00 eV, T_1 -2.65 eV).

Acknowledgment. We thank the National Science Foundation for their generous support of this research.

Supporting Information Available: Synthesis, computational data, X-ray, and ESR. This material is available free of charge via the Internet at <http://pubs.acs.org>.

OL802763R